Title

Charge neutralization in the active site of the catalytic trimer of aspartate transcarbamoylase promotes diverse structural changes.

Journal

Protein Science, 26(11)

Authors

Endrizzi, James
Beernink, Peter

Publication Date

2017-11-01

DOI

10.1002/pro.3277

Peer reviewed

THE PROTEIN SOCIETY

Charge neutralization in the active site of the catalytic trimer of aspartate transcarbamoylase promotes diverse structural changes

James A. Endrizzi[1] and Peter T. Beernink[2,3]*

[1]Supernova C, Missoula, Montana

[2]Children's Hospital Oakland Research Institute, UCSF Benioff Children's Hospital, Oakland, California

[3]Department of Pediatrics, School of Medicine, University of California, San Francisco, San Francisco, California

Received 30 June 2017; Accepted 14 August 2017
DOI: 10.1002/pro.3277
Published online 19 August 2017 proteinscience.org

Abstract: A classical model for allosteric regulation of enzyme activity posits an equilibrium between inactive and active conformations. An alternative view is that allosteric activation is achieved by increasing the potential for conformational changes that are essential for catalysis. In the present study, substitution of a basic residue in the active site of the catalytic (C) trimer of aspartate transcarbamoylase with a non-polar residue results in large interdomain hinge changes in the three chains of the trimer. One conformation is more open than the chains in both the wild-type C trimer and the catalytic chains in the holoenzyme, the second is closed similar to the bisubstrate-analog bound conformation and the third hinge angle is intermediate to the other two. The active-site 240s loop conformation is very different between the most open and closed chains, and is disordered in the third chain, as in the holoenzyme. We hypothesize that binding of anionic substrates may promote similar structural changes. Further, the ability of the three catalytic chains in the trimer to access the open and closed active-site conformations simultaneously suggests a cyclic catalytic mechanism, in which at least one of the chains is in an open conformation suitable for substrate binding whereas another chain is closed for catalytic turnover. Based on the many conformations observed for the chains in the isolated catalytic trimer to date, we propose that allosteric activation of the holoenzyme occurs by release of quaternary constraint into an ensemble of active-site conformations.

Keywords: allosteric enzyme; ATCase; conformational changes; crystal structure; flexibility; interdomain hinge

Abbreviations: Asp, aspartate; ATCase, aspartate transcarbamoylase; C, catalytic (subunit or trimer); CbmP, carbamoyl phosphate; NCS, non-crystallographic symmetry; PALA, N-phosphonacetyl-L-aspartate; WT, wild-type.

Importance: One of the paradigms for allosteric enzyme regulation, aspartate transcarbamoylase, previously had been observed only in three-fold symmetric structures. Our studies of the isolated catalytic trimer identified significant deviations from threefold symmetry and this asymmetry is even more pronounced when the positively charged active sites are partially neutralized by an amino acid substitution. The opposing hinge angle changes seen in this mutant suggest that conformational changes necessary for substrate binding and catalysis are linked.

Grant sponsor: Office of Extramural Research, National Institutes of Health (NIH) National Institute of General Medical Sciences (NIGMS); Grant numbers: R01 GM 12159 (HKS), R01 GM 54793 (TCA) and F32 GM 19014 (PTB).

*Correspondence to: Peter T. Beernink, Children's Hospital Oakland Research Institute, UCSF Benioff Children's Hospital, Oakland, California. E-mail: pbeernink@chori.org

Introduction

Since the pioneering crystallographic studies on yeast hexokinase,[1] carboxypeptidase A[2] and T4 lysozyme,[3] hinge-bending motions in enzymes have been recognized as important for catalysis. Other examples of hinge closure upon substrate binding include phosphoglycerate kinase,[4] gluconate kinase,[5] and angiotensin converting enzyme-related carboxypeptidase, ACE2.[6] These conformational changes have been interpreted as supporting the "induced-fit" theory of enzyme activity.[7,8]

An alternative, but not mutually exclusive, theory coined "conformational selection" proposes that enzymes preexist in an ensemble of states, and that substrates preferentially bind to a subset of these enzyme conformations.[9] This conformational ensemble can be viewed as analogous to those in the protein folding landscape.[10] Experimental evidence for multiple conformational states in the absence of substrates include NMR relaxation studies of the prolyl *cis-trans* isomerase cyclophilin A, which show that characteristic conformational changes during catalysis also occur in the free enzyme.[11]

Conformational changes upon substrate binding also have been observed for many allosteric enzymes such as lactate dehydrogenase,[12] phosphofructokinase,[13,14] CTP synthetase[15,16] and aspartate transcarbamoylase (ATCase). In ATCase, the tertiary structural changes include domain closure in the catalytic (C) chains, which is thought to be linked to the quaternary structural changes in the dodecameric enzyme.[17] The structures of ATCase holoenzymes in free[18,19] and bisubstrate analog bound states[20] display three-fold crystallographic symmetry and near two-fold symmetry. The release of structural constraints from the taut- (T-) state holoenzyme previously was proposed to explain the allosteric activation of the enzyme,[21] which is consistent with the concerted allosteric model of Monod et al.[22] In contrast, the structure of the isolated C trimer exhibits asymmetry in its interdomain hinge conformations.[21] The inferred flexibility of the isolated C trimer contrasts with the quaternary constraint of the C trimer when assembled into the holoenzyme. This increased flexibility was hypothesized to explain the higher catalytic activity of the C trimer compared with the relaxed- (R-) state enzyme.[21]

In the present study, we determined the high-resolution crystal structure of a mutant C trimer of ATCase, which contains a single amino acid replacement of arginine by alanine (R105A) in the carbamoyl-phosphate (CbmP) binding site. This substitution decreases the activity of the holoenzyme by 1100-fold and decreases the apparent affinity for the substrate CbmP by 35-fold.[23] We infer that large tertiary structural changes in the mutant C trimer result from neutralization of a single active site charge and that the opposite conformational changes in the hinge angles of different chains indicate that the tertiary conformations within the trimer are linked energetically.

Table I. X-Ray Data Collection and Refinement Statistics[a]

Crystals	
Space group	$P2_12_12_1$
Unit cell dimensions (Å)	
a	56.03
b	81.10
c	211.65
V_m (Å^3/Da)	2.34
Data	
Resolution range (Å)	18.29–2.01
Unique/measured reflections	57,740/190,953
Completeness (%):	89.8 (82.0)
Average I/σI	11.7 (2.9)
R_{sym} (%)	0.071 (0.353)
Refinement	
R_{cryst}	0.175
R_{free}	0.227
RMS Deviations	
Bond lengths (Å)	0.007
Bond angles (°)	0.87
Planar groups (Å)	0.005
Φ/Ψ Most Favored (%)	97.5

[a] values in parentheses are for the 2.06 to 2.01-Å resolution shell.

Results

Structure of the R105A mutant C trimer

We determined the structure of the R105A mutant C trimer to 2.0-Å resolution by molecular replacement using the structure of the wild-type C trimer (PDB ID 3CSU)[21] as a search model. The structure was refined to a crystallographic R factor of 0.175 and a free R factor of 0.227 with good geometry (Table I). Most of the residues (897 of 930) in the three polypeptide chains exhibit well-defined electron density; the ranges of the residues present in the model are provided in Table II. The site of the R105A substitution has electron density that is consistent with the presence of an alanine side chain and a feature-enhanced[24] omit map confirms the presence of the substitution (Fig. 1).

The most distinctive structural feature of the R105A mutant C trimer is the asymmetry in the relative orientations of the two domains within each of the three catalytic chains. Since the tertiary structural differences primarily involve rotation of one domain with respect to the other, the two domains can be viewed as being related by a hinge, with various angular differences between conformations. After superimposing one of the two structural domains of each chain, large differences are seen in the relative positions of the other domain among the three chains [Fig. 2(A)], which differ by as much as 14.4° (Table II).

Table II. *Interdomain Hinge Angle Comparisons of C Trimer Conformations Compared to the Closed, ATCase-PALA Conformation*

Assembly (sequence, ligand)	PDB ID (Chain ID)	Hinge angle difference (°)[a]
C trimer (R105A, none)[b]	5VMQ (A)	14.4
	5VMQ (B)	9.3
	5VMQ (C)	0.2
C trimer (WT, none)[21]	3CSU (A)	12.0
	3CSU (B)	8.5
	3CSU (C)	6.3
C trimer (WT, PALA)[25]	1EKX (A)	0.2
Holoenzyme (WT, none)[18]	6AT1 (A)	5.9

[a] The hinge angle difference (in degrees) is relative to the most closed known conformation (ATCase-PALA; PDB entry 1D09, chain A)[26]. Hinge angle differences were calculated as described in Methods.

[b] Electron density was observed in chain A for residues 1–77, 85–128, 134–310 (of 310); in chain B for residues 2–231, 247–305; and in chain C for residues 1–310.

Two active-site loops, the 80s and 130s loops, exhibit low electron density in one of the chains (A), and the 240s loop displays low density in another chain (B), which indicates that their conformations are disordered [represented by gaps in the Cα traces in Fig. 2(A)]. For the active-site loops that exhibit well-defined electron density, their conformations are variable. A noteworthy example is the 240s loop, which is reoriented by 21° in chain C relative to chain A [Fig. 2(A)]. Progressively smaller differences in loop conformations are evident in the 130s, 80s, and 50s loops [Fig. 2(A)]. Following superposition of the amino-terminal domain of each chain, a plot of the difference in the alpha carbon (Cα) position for each residue depicts the relative displacement of the

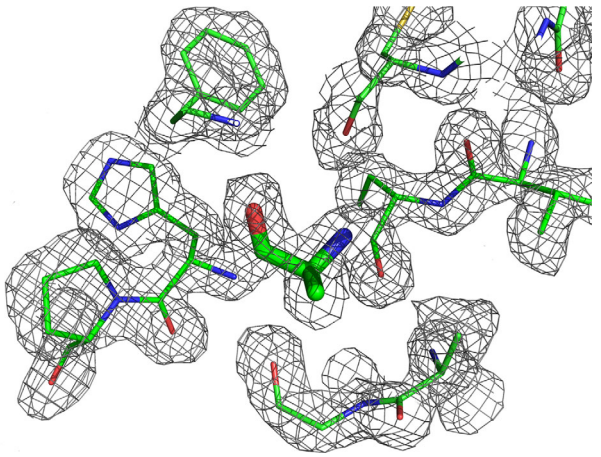

Figure 1. Feature-enhanced electron density map[24] of the active-site region containing the R105A substitution with residue A105 omitted from the map calculation. The map, which is shown at a contour level of 1.0σ, shows density consistent with an alanine residue at position 105, which is shown in a thicker stick representation. The map was generated using PHENIX[27,28] and the figure was rendered using PyMOL (https://www.pymol.org)

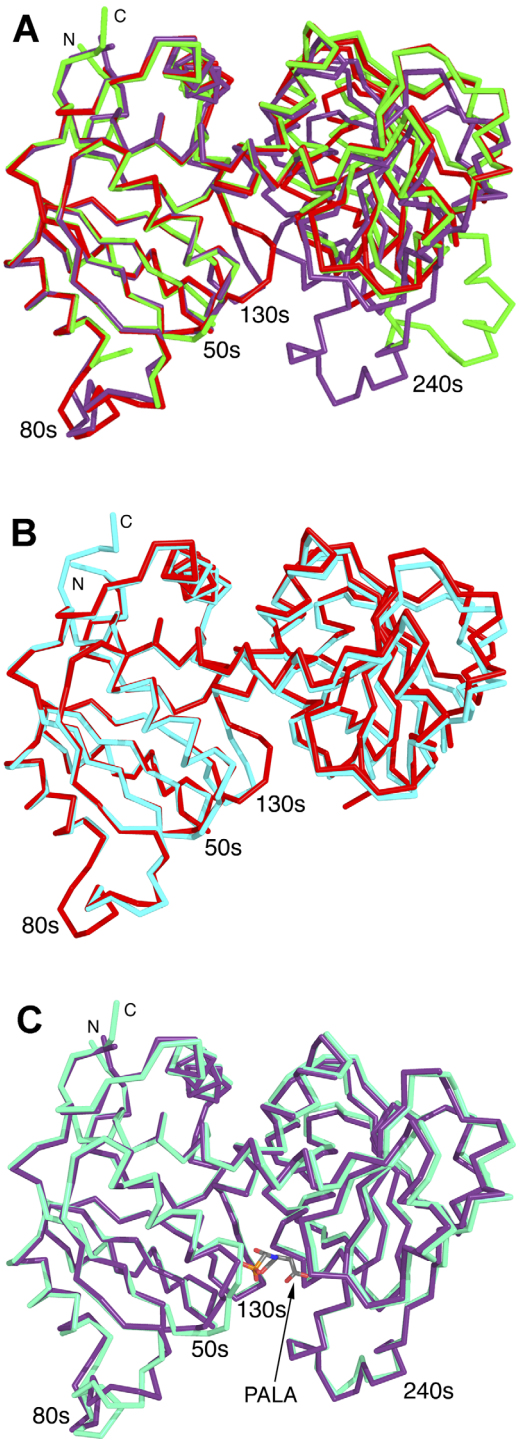

Figure 2. Hinge differences among chains of the R105A mutant C trimer. The chains were superimposed based on N-terminal domain residues 1–73 and 90–134 and the hinge differences can be seen from the relative displacement of C-terminal domains. **A,** Comparison of the three chains in the R105A mutant C trimer. The chains are shown as Cα traces; chain A, green; B, red; and C, violet. **B,** Comparison of the R105A mutant C trimer (chain B, red) to the wild-type C trimer (chain B, light blue)[21] shows the intermediate hinge conformations of the two structures. The 240s loop, which is disordered in both chains, is not depicted. **C,** Comparison of the most closed chain conformation of the R105A mutant C trimer (chain C, violet) with a chain from the C trimer-PALA complex (1EKX)[25] (chain C, light green)

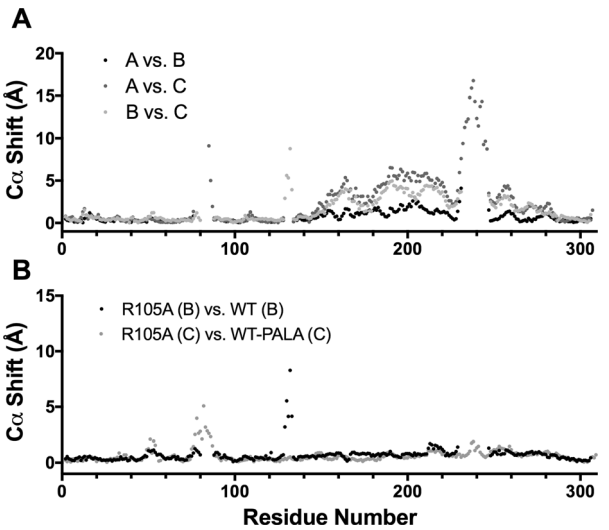

Figure 3. Hinge differences or similarities as shown from plots of pairwise Cα differences. The chains were superimposed based on N-terminal domain residues 1–73 and 90–134 and the hinge differences can be seen from the relative displacement of C-terminal domains. **A,** Pairwise differences among the three chains in the R105A mutant C trimer. Chain A vs. B, black symbols; chain A vs. C, dark grey symbols; chain B vs. C, light grey symbols. Comparisons correspond to the superpositions shown in Figure 2(A). **B,** Pairwise differences between the R105A mutant C trimer (chain B) and WT C trimer (chain B)[21], black symbols, and between the R105A mutant C trimer (chain C) and C trimer-PALA (chain C)[25], grey symbols. Comparisons correspond to the superpositions shown in Figure 2(B,C)

carboxyl-terminal domain, as well as the differences in local conformations for the three chains [Fig. 3(A)].

Comparison to wild-type C trimer and holoenzyme structures

The structure of the R105A mutant C trimer is asymmetric in its hinge conformations, with differences of up to 14.4°. These differences are considerably greater than those observed in the wild-type C trimer, which differ by up to 5.7°.[21] One of the chains in the R105A mutant C trimer (chain A) is 2.4° more open than the most open chain (A) of the wild-type C trimer (Table II). The second (chain B) is slightly more open (0.8°) than the intermediate conformation (chain B) of the wild-type C trimer. The most closed chain of the R105A mutant C trimer (chain C) is 6.1° more closed than the corresponding chain of the C trimer (C). The hinge conformation of chain C of the R105A mutant trimer is nearly identical (0.2° more open) to all three chains in the structure of the C trimer in a complex with the bisubstrate analog PALA[25] (Table II). This result is surprising since the bisubstrate analog tethers the two domains of each chain in a closed conformation in the C trimer-PALA complex.[25] Further, all of the previously determined ATCase structures without active-site ligands (e.g., [18,19,21]) display relatively open hinge conformations.

Like the wild-type C trimer, the R105A mutant C trimer contains disordered active-site loops. However, the locations of the disordered loops, and the number of each, differ between the two structures. For example, the 80s loop is disordered in one chain (A) of the R105A mutant C trimer, whereas this loop is disordered in all three chains of the wild-type C trimer[21]. The 130s loop is disordered in one chain (A) of the R105A trimer, but is ordered in all three chains of the wild-type C trimer. The 240s loop is disordered in one chain (B) of the R105A trimer, compared with two chains in the wild-type C trimer. In contrast to the wild-type and mutant C trimers, all of the active-site loops in the C trimer-PALA complex are ordered because these loops directly contact the bisubstrate analog. In all of the known C trimer structures, the 240s loop either is disordered or adopts one of two ordered conformations, which differ in orientation relative to the remainder of the carboxyl-terminal domain by 21° [Fig. 2(A)]. Two of the three chains of the R105A mutant C trimer exhibit significant differences in loop positions compared to both the wild-type C trimer and its complex with PALA.

The third chain (C) of the R105A mutant C trimer, which resembles the closed conformation of the C trimer-PALA complex in its interdomain conformation, also resembles the latter in several of its active-site loop conformations [Fig. 2(C)]. Whereas the 240s loop of chain C is quite similar to that in the C trimer-PALA complex, the 80s loops differ by as much as 5 Å in their respective Cα positions [Fig. 3(B)]. Most of the active-site residues adopt conformations that are similar to those in the presence of bound PALA (Fig. 4). A noteworthy exception is the side chain of Arg54, which occupies a position that sterically occludes the active site. The side chain of Arg54 makes several hydrogen bonds with neighboring residues; Arg54 NH1 and NH2 are positioned 3.0 and 3.5 Å, respectively, from the carbonyl oxygen of Leu267, and Arg54 NH2 is 3.0 Å from Gln137 NE2. The interaction between Arg54 and Leu267, which are in different structural domains, appears to stabilize the closed hinge conformation in the absence of bound substrates or analogs.

The structure of the R105A mutant ATCase holoenzyme (PDB ID 1I5O)[29] closely resembles the structure of non-liganded ATCase (PDB ID 6AT1)[18], except at the site of the residue substitution. Therefore, we compared the structure of the R105A mutant C trimer to non-liganded ATCase, whose structure had been determined to a higher resolution limit than the R105A mutant holoenzyme. The hinge conformations of the R105A mutant C trimer range from 9° more open (chain A) to 6° more closed (chain C) than the catalytic chains in the free ATCase holoenzyme. The active-site loops that are disordered in the R105A mutant C trimer are

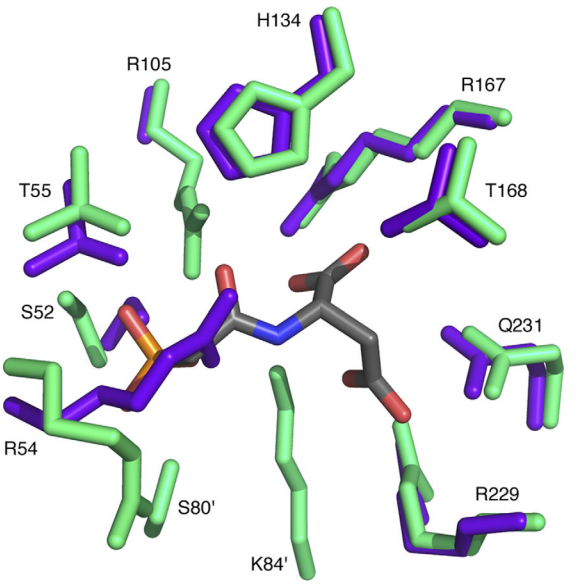

Figure 4. Differences in active site residues in the most closed chain of the R105A mutant C trimer (chain C, violet) and a chain from the C trimer-PALA complex (chain C, light green) (1EKX).[25] Chains were superimposed using the backbone atoms of all residues. Known substrate binding residues are shown. Residues S80 and K84 (denoted with prime (′) are contributed by an adjacent chain (A) and are disordered in this chain of the R105 mutant C trimer. The bisubstrate analog from the C trimer-PALA complex is shown at the center in dark gray. The side chain of Arg54 in chain C of the R105A mutant occupies the PALA-binding site and mediates domain-bridging interactions, which stabilizes the closed conformation in the absence of substrates

ordered in the wild-type and R105A holoenzymes due to interchain contacts not present in the C trimer. Specifically, in the holoenzyme, the 130s loop contacts a catalytic chain from the apposing trimer, the 240s loop contacts apposing catalytic and regulatory chains and the 80s loop contacts an adjacent catalytic chain. Since the C trimers in the ATCase-PALA complex (6AT1)[18] and (1D09)[26] closely resemble the C trimer-PALA complex (1EKX)[25] described above, separate comparisons between the R105A mutant C trimer and the ATCase-PALA complex did not yield any additional insights.

Discussion

It is noteworthy that a T4 lysozyme mutant with a substitution between the two structural domains previously was observed in five different conformations, with interdomain hinge displacements of up to 32°.[3] In our previous study, the wild-type ATCase catalytic trimer exhibited three different conformations[21] and a fourth conformation was seen in the presence of a bisubstrate analog,[25] with hinge differences as large as 12°. In the present study, we observe two new conformations in an ATCase catalytic trimer mutant, which possesses a substitution, R105A, in the active-site cleft between the two domains. For both lysozyme and C trimer mutants, the observations of multiple conformations are interpreted to represent flexibility of the enzymes in solution.

In the structure of the wild-type C trimer,[21] R105 mediates polar interactions with the side chains of residues E50 and S52, and with the backbone carbonyl oxygen atoms of A127 and G130. Since R105 is in the amino-terminal domain and does not contact residues in the carboxyl-terminal domain (residues 150–284, see Methods), we infer that the large and diverse structural changes in the R105A mutant C trimer are attributable to partial neutralization of positive charge in the active site. Collectively, the R105A mutant C trimer and the previously described structure of the wild-type C trimer exhibit six different interdomain hinge conformations. This structural variation suggests that the C trimer is flexible in solution[21] and that charge neutralization in the active site, either by mutagenesis as described here, or naturally by deprotonation of basic residues, binding of substrates or other ions in the active sites can lead to large conformational changes.

It is striking that the same substitution led to opposite conformational changes in the hinge angle between domains in two of the chains in the mutant C trimer relative to the wild-type C trimer. This observation suggests that the conformational changes are structurally and energetically linked. The asymmetry in the two structures and the opposing hinge changes in R105A mutant C trimers may explain previous observations of functional heterogeneity in the active sites of the wild-type C trimer with respect to binding the first substrate CbmP[30]. Moreover, the bisubstrate analog PALA bound to the wild-type C trimer with a stoichiometry of 2.3 PALA per C trimer in two independent studies.[31,32] Although the high-resolution crystal structure of the C trimer in a complex with PALA shows three molecules of PALA bound with full occupancy[25], another crystal structure was obtained with two PALA molecules bound and all three hinges were in the closed conformation (authors' unpublished data). Therefore, the stoichiometry of 2.3 PALA bound per C trimer suggests that either two or three PALA can bind the wild-type C trimer and that binding of the third PALA molecule might depend on the kinetics of the associated conformational changes.

Interestingly, in an earlier study, hybrid ATCase holoenzymes containing the R105A substitution in five of the six catalytic chains were used to assess the structural effects of PALA binding to one of the six catalytic chains by small-angle X-ray scattering.[29] Surprisingly, the conformational changes seen in the R105A mutant C trimer were not seen in the crystal structure of the R105A holoenzyme, which resembled the free, T-state holoenzyme[29]. This result reinforces the earlier proposal that the assembly of C trimers into holoenzyme imposes symmetry[21].

In summary, the marked asymmetry of the R105A mutant C trimer, in contrast to the moderate asymmetry of the wild-type C trimer, shows that large conformational changes likely result from neutralization of a single active-site charge. The potential for large conformational changes promoted by neutralization of an active-site charge suggests that the catalytic chains likely access multiple conformations during a catalytic cycle, including open conformations that allow substrate binding and/or product release, and a closed conformation for transition-state stabilization. Furthermore, the potential for these conformations to be coupled suggests that catalytic turnover may occur among the three active sites in an alternating, or cyclic, fashion. Although the potential for conformational changes is likely to be lower in the more constrained holoenzyme[21], catalysis in ATCase likely depends on similar sampling of multiple conformational states during a catalytic cycle. The proposal that allosteric activation in the ATCase holoenzyme occurs through the release of structural constraints into an ensemble of conformations will require further structural studies, including those on mutant ATCase enzymes whose equilibrium favors the activated R-state.

Materials and Methods

Site-specific mutagenesis

The R105A substitution was introduced into the *E. coli pyrB* gene by PCR mutagenesis.[33] Two overlapping fragments were generated, each using one primer that flanked the gene and one mutagenic primer. The forward and reverse mutagenic oligonucleotide sequences were: 5′ CGATAGTGATGGCT CATCCGCAGG and 5′ CCTGCGGATGAGCCATCAC TATCG, respectively. The overlapping fragments were mixed in an equimolar ratio and the mutant *pyrB* gene was amplified using the flanking primers. The PCR product was digested with the restriction endonucleases *Nco*I and *Hind*III and ligated into the ATCase expression plasmid pAX4, which was derived from pRCP000.[34]

Protein purification and crystallization

ATCase containing the R105A substitution in the catalytic chains and a His_6 sequence at the N-terminus of each regulatory chain was purified as previously described for ATCase His_6 enzyme.[34] Mutant C subunits were isolated from the His_6-tagged holoenzyme by treatment with neohydrin followed by ion exchange chromatography.[35] Orthorhombic crystals of the C_{R105A} mutant trimer were obtained by vapor diffusion at 4°C from hanging drops containing 5 μL 0.1 M Tris-HCl, pH 7.8, 0.04 M CaOAc, 7.5% PEG 8000 and 5 μL of C subunit (6.1 mg/mL) in 10 mM Tris-HCl, pH 7.5, 1 mM 2-mercaptoethanol. The crystals grew in space group $P2_12_12_1$, with unit cell dimensions $a = 56.03$, $b = 81.10$, $c = 211.65$ Å (Table I).

Structure determination and refinement

Crystals (ca. 1.0 × 0.3 × 0.2 mm) were equilibrated to 40 mM Tris·Cl, pH 7.5, 40 mM CaOAc, 29% PEG 8000, 22% methylpentanediol and flash cooled on a 0.1 mm nylon loop (Hampton Research) in liquid N_2. The X-ray data were collected from a single crystal at 100 K using a Mar345 image plate on beam line 7–1 at the Stanford Synchrotron Radiation Laboratory. The data were integrated and scaled using MOSFLM[36] and SCALA[37] to give $R_{sym} = 0.071$ for 57,740 independent reflections from 20.0–2.0-Å resolution. The data were 90% complete overall, with average $I/\sigma I$ values of 11.7 (2.9 in the 2.06–2.01 Å shell; Table I). Molecular replacement was carried out with AMoRe[38] using the structure of the wild-type C trimer[21] as a search model.

Rigid-body refinement of individual domains was followed by positional and restrained B factor refinement using TNT.[39] Further stages of refinement were performed with refmac[40] and phenix.refine[27] using three-fold non-crystallographic symmetry (NCS) restraints for each of the two structural domains. Model building was carried out using XtalView[41] and Coot.[42] Iterations of refinement and manual building were carried out until the R_{free} converged. The NCS restraints were relaxed at the end of refinement, which resulted in a slight decrease in R_{free}. The final model contains 6988 protein atoms in three polypeptide chains, 429 water molecules, one Ca^{2+} and one Cl^- ion. The structure has been refined to a crystallographic R factor of 0.175, a free R factor of 0.227 with good geometry (Table I). Ninety-eight percent of residues are in the favored regions of a Ramachandran plot and only the arginine at position 270 occupies a disallowed region, as has been observed in other high-resolution ATCase structures.[21,26] The atomic coordinates and structure factors have been deposited in the Protein Data Bank (http://www.rcsb.org; accession number 5VMQ).

Structural analysis

Superpositions and hinge angle calculations were performed using GEM.[43] Hinge angle differences were calculated as the rotation angle required to bring an amino-terminally superimposed pair of molecules into carboxyl-terminal superposition. Superpositions were based on residues comprising the amino-terminal (1–73 and 90–134) or carboxyl-terminal (150–229 and 252–284) domains and excluded the two interdomain helices (135–149 and 285–305) and two variable active-site loops (residues 74–89 and 230–251). Active-site comparisons were done based on backbone atom superpositions of entire chains. Structural superpositions and figures

were generated using PyMOL (https://www.pymol.org).

Acknowledgments

We acknowledge Professors Howard K. Schachman and Thomas C. Alber (U.C. Berkeley) posthumously for financial support. We thank Daniel E. Koshland posthumously for engaging discussions.[44] This research was supported by National Institutes of Health (NIH) National Institute of General Medical Sciences (NIGMS) Research Grants R01 GM 12159 (HKS), R01 GM 54793 (TCA), and National Research Service Award F32 GM 19014 to PTB. Use of the Stanford Synchrotron Radiation Lightsource (SSRL), SLAC National Accelerator Laboratory, is supported by the U.S. Department of Energy (DOE), Office of Science, Office of Basic Energy Sciences under Contract No. DE-AC02–76SF00515. The SSRL Structural Molecular Biology Program is supported by the DOE Office of Biological and Environmental Research, and by the NIH, NIGMS (including P41 GM 103393). The contents of this publication are solely the responsibility of the authors and do not necessarily represent the official views of NIGMS or NIH. The authors declare no conflicts of interest.

References

1. Bennett WS, Jr, Steitz TA (1978) Glucose-induced conformational change in yeast hexokinase. Proc Natl Acad Sci USA 75:4848–4852.
2. Rees DC, Lipscomb WN (1981) Binding of ligands to the active site of carboxypeptidase A. Proc Natl Acad Sci USA 78:5455–5459.
3. Faber HR, Matthews BW (1990) A mutant T4 lysozyme displays five different crystal conformations. Nature 348:263–266.
4. Bernstein BE, Hol WG (1998) Crystal structures of substrates and products bound to the phosphoglycerate kinase active site reveal the catalytic mechanism. Biochemistry 37:4429–4436.
5. Kraft L, Sprenger GA, Lindqvist Y (2002) Conformational changes during the catalytic cycle of gluconate kinase as revealed by X-ray crystallography. J Mol Biol 318:1057–1069.
6. Towler P, Staker B, Prasad SG, Menon S, Tang J, Parsons T, Ryan D, Fisher M, Williams D, Dales NA, et al. (2004) ACE2 X-ray structures reveal a large hinge-bending motion important for inhibitor binding and catalysis. J Biol Chem 279:17996–18007.
7. Koshland DE (1994) The key-lock theory and the induced fit theory. Angew Chem Inl Ed Engl 33:2375–2378.
8. Herschlag D (1988) The role of induced fit and conformational changes of enzymes in specificity and catalysis. Bioorg Chem 16:62–96.
9. Bahar I, Chennubhotla C, Tobi D (2007) Intrinsic dynamics of enzymes in the unbound state and relation to allosteric regulation. Curr Opin Struct Biol 17:633–640.
10. Frauenfelder H, Sligar SG, Wolynes PG (1991) The energy landscapes and motions of proteins. Science 254:1598–1603.
11. Eisenmesser EZ, Millet O, Labeikovsky W, Korzhnev DM, Wolf-Watz M, Bosco DA, Skalicky JJ, Kay LE, Kern D (2005) Intrinsic dynamics of an enzyme underlies catalysis. Nature 438:117–121.
12. Iwata S, Ohta T (1993) Molecular basis of allosteric activation of bacterial L-lactate dehydrogenase. J Mol Biol 230:21–27.
13. Shirakihara Y, Evans PR (1988) Crystal structure of the complex of phosphofructokinase from *Escherichia coli* with its reaction products. J Mol Biol 204:973–994.
14. Rypniewski WR, Evans PR (1989) Crystal structure of unliganded phosphofructokinase from *Escherichia coli*. J Mol Biol 207:805–821.
15. Endrizzi JA, Kim H, Anderson PM, Baldwin EP (2004) Crystal structure of *Escherichia coli* cytidine triphosphate synthetase, a nucleotide-regulated glutamine amidotransferase/ATP-dependent amidoligase fusion protein and homologue of anticancer and antiparasitic drug targets. Biochemistry 43:6447–6463.
16. Endrizzi JA, Kim H, Anderson PM, Baldwin EP (2005) Mechanisms of product feedback regulation and drug resistance in cytidine triphosphate synthetases from the structure of a CTP-inhibited complex. Biochemistry 44:13491–13499.
17. Lipscomb WN, Kantrowitz ER (2012) Structure and mechanisms of *Escherichia coli* aspartate transcarbamoylase. Acc Chem Res 45:444–453.
18. Stevens RC, Gouaux JE, Lipscomb WN (1990) Structural consequences of effector binding to the T state of aspartate carbamoyltransferase: crystal structures of the unligated and ATP- and CTP-complexed enzymes at 2.6-A resolution. Biochemistry 29:7691–7701.
19. Stieglitz KA, Xia J, Kantrowitz ER (2009) The first high pH structure of *Escherichia coli* aspartate transcarbamoylase. Proteins 74:318–327.
20. Krause KL, Volz KW, Lipscomb WN (1987) 2.5 Å structure of aspartate carbamoyltransferase complexed with the bisubstrate analog *N*-(phosphonacetyl)-L-aspartate. J Mol Biol 193:527–553.
21. Beernink PT, Endrizzi JA, Alber T, Schachman HK (1999) Assessment of the allosteric mechanism of aspartate transcarbamoylase based on the crystalline structure of the unregulated catalytic subunit. Proc Natl Acad Sci USA 96:5388–5393.
22. Monod J, Wyman J, Changeux J-P (1965) On the nature of allosteric transitions: A plausible model. J Mol Biol 12:88–118.
23. Stebbins JW, Xu W, Kantrowitz ER (1989) Three residues involved in binding and catalysis in the carbamyl phosphate binding site of *Escherichia coli* aspartate transcarbamylase. Biochemistry 28:2592–2600.
24. Afonine PV, Moriarty NW, Mustyakimov M, Sobolev OV, Terwilliger TC, Turk D, Urzhumtsev A, Adams PD (2015) FEM: feature-enhanced map. Acta Cryst D71: 646–666.
25. Endrizzi JA, Beernink PT, Alber T, Schachman HK (2000) Binding of bisubstrate analog promotes large structural changes in the unregulated catalytic trimer of aspartate transcarbamoylase: implications for allosteric regulation. Proc Natl Acad Sci USA 97: 5077–5082.
26. Jin L, Stec B, Lipscomb WN, Kantrowitz ER (1999) Insights into the mechanisms of catalysis and heterotropic regulation of *Escherichia coli* aspartate transcarbamoylase based upon a structure of the enzyme complexed with the bisubstrate analogue N-phosphonacetyl-L-aspartate at 2.1 A. Proteins 37:729–742.
27. Afonine PV, Grosse-Kunstleve RW, Echols N, Headd JJ, Moriarty NW, Mustyakimov M, Terwilliger TC,

Urzhumtsev A, Zwart PH, Adams PD (2012) Towards automated crystallographic structure refinement with phenix.refine. Acta Cryst D68:352–367.
28. Adams PD, Afonine PV, Bunkoczi G, Chen VB, Davis IW, Echols N, Headd JJ, Hung LW, Kapral GJ, Grosse-Kunstleve RW, et al. (2010) PHENIX: a comprehensive Python-based system for macromolecular structure solution. Acta Cryst D66:213–221.
29. Macol CP, Tsuruta H, Stec B, Kantrowitz ER (2001) Direct structural evidence for a concerted allosteric transition in *Escherichia coli* aspartate transcarbamoylase. Nat Struct Biol 8:423–426.
30. Suter P, Rosenbusch JP (1976) Heterogeneity of sites in isolated catalytic subunits of aspartate transcarbamoylase. Eur J Biochem 70:191–196.
31. Newell JO, Markby DW, Schachman HK (1989) Cooperative binding of the bisubstrate analog *N*-(phosphonacetyl)-L-aspartate to aspartate transcarbamoylase and the heterotropic effects of ATP and CTP. J Biol Chem 264:2476–2481.
32. Foote J, Schachman HK (1985) Homotropic effects in aspartate transcarbamoylase: What happens when the enzyme binds a single molecule of the bisubstrate analog *N*-phosphonacetyl-L-aspartate? J Mol Biol 186: 175–184.
33. Sambrook J, Fritch EF, Maniatis T (1989) Molecular cloning: a laboratory manual. Cold Spring Harbor, NY: Cold Spring Harbor Laboratory Press.
34. Graf R, Schachman HK (1996) Random circular permutation of genes and expressed polypeptide chains: Application of the method to the catalytic chains of aspartate transcarbamoylase. Proc Natl Acad Sci USA 93:11591–11596.
35. Yang YR, Kirschner MW, Schachman HK (1978) Aspartate transcarbamoylase (*Escherichia coli*): Preparation of subunits. Methods Enzymol 51:35–41.
36. Battye TG, Kontogiannis L, Johnson O, Powell HR, Leslie AG (2011) iMOSFLM: a new graphical interface for diffraction-image processing with MOSFLM. Acta Cryst D67:271–281.
37. Winn MD, Ballard CC, Cowtan KD, Dodson EJ, Emsley P, Evans PR, Keegan RM, Krissinel EB, Leslie AG, McCoy A, et al. (2011) Overview of the CCP4 suite and current developments. Acta Cryst D67:235–242.
38. Navaza J (1994) AMoRe: an automated package for molecular replacement. Acta Cryst A50:157–163.
39. Tronrud DE, Ten Eyck LF, Matthews BW (1987) An efficient general-purpose least-squares refinement program for macromolecular structures. Acta Cryst A43: 489–501.
40. Murshudov GN, Skubak P, Lebedev AA, Pannu NS, Steiner RA, Nicholls RA, Winn MD, Long F, Vagin AA (2011) REFMAC5 for the refinement of macromolecular crystal structures. Acta Cryst D67:355–367.
41. McRee DE (1992) XtalView: a visual protein crystallographic software system for X11/XView. J Mol Graphics 10:44–47.
42. Emsley P, Lohkamp B, Scott WG, Cowtan K (2010) Features and development of Coot. Acta Cryst D66:486–501.
43. Fauman EB, Rutenber EE, Maley GF, Maley F, Stroud RM (1994) Water-mediated substrate/product discrimination: the product complex of thymidylate synthase at 1.83 A. Biochemistry 33:1502–1511.
44. Koshland DE (2004) Crazy but correct: How a non-conformist theory beat scepticism and got into the textbooks. Nature 432:447.